Accounting for vegetation height and wind direction to correct eddy covariance measurements of energy fluxes over hilly crop fields

Rim Zitouna, Frédéric Jacob, Marc Voltz, Laurent Prevot

Accounting for vegetation height and wind direction to correct eddy covariance measurements of energy fluxes over hilly crop fields

Rim Zitouna-Chebbi, INRGREF – Carthage University, Tunis, Tunisia

Laurent Prévot, INRA – UMR LISAH, Montpellier, France

Frédéric Jacob, IRD – UMR LISAH, Montpellier, France

Marc Voltz, INRA – UMR LISAH, Montpellier, France

Corresponding author: R. Zitouna-Chebbi, INRGREF – Carthage University, BP N°10, Ariana 2080, Tunisia. (rimzitouna@gmail.com)

Key Points

Eddy covariance measurements are collected over rainfed hilly crop fields

Airflow inclination depends upon upslope / downslope winds and crop height

Tilt corrections are adjusted accordingly, and improve energy balance closure

Abstract: As agricultural hilly watersheds are widespread throughout the world, there is as strong need for reliable estimates of land surface fluxes, especially evapotranspiration, over crop fields on hilly slopes. In order to obtain reliable estimates from eddy covariance (EC) measurements in such conditions, the current study aimed at proposing adequate planar fit tilt corrections that account for the combined effects of topography, wind direction and vegetation height on airflow inclinations. EC measurements were collected within an agricultural hilly watershed in northeastern Tunisia, throughout the growth cycles of cereals, legumes and pasture. The wind had two dominant directions that induced upslope and downslope winds. For upslope winds, the airflows were parallel to the slopes and slightly came closer to the horizontal plane when vegetation grew. For downslope winds, over fields located in the lee of the rim top, the airflows were almost horizontal over bares soils and came closer to the topographical slope when vegetation grew. We therefore adjusted the planar fit tilt correction on EC measurements according to vegetation height and by discriminating between upslope and downslope winds. This adjusted tilt correction improved the energy balance closure in most cases, and the obtained energy balance closures were similar to that reported in the literature for flat conditions. We conclude that EC data collected within crop fields on hilly slopes can be used for monitoring land surface fluxes, provided planar fit tilt corrections are applied in an appropriate manner.

***Keywords**:* Eddy covariance measurements; Hilly slopes; Agricultural canopies; Airflow inclination; Planar fit tilt correction; Energy balance closure

1. Introduction

Knowledge of land surface momentum, mass and energy fluxes is of strong interest for documenting land surface boundary conditions in meteorology [Boone et al., 2009; Steeneveld et al., 2011], soil surface and subsurface moisture in hydrology [Gómez-Delgado et al., 2011; Cai et al., 2014], and crop water consumption in agriculture [Abedinpour et al., 2012; Zeri et al., 2013]. Among land surface fluxes, latent heat flux, or evapotranspiration, is critical under sub-humid and semi-arid climates since it corresponds to up to 80% of the yearly hydrological budget [Moussa et al., 2007]. Over the last decades, work on observing and modeling land surface fluxes were mainly focused on flat landscapes with sparse or full covering canopies [e.g., Courault et al., 2005; Kalma et al., 2008; Allen et al., 2011; Wang and Dickinson, 2012; Chen et al., 2013; Kool et al., 2014].

Agricultural hilly watersheds are common in many parts of the world [Zhang et al., 2004; Mishra et al., 2008; Khlifi et al., 2010; Maeda et al., 2010]. They experience agricultural intensification, because hilly topographies allow water-harvesting techniques that compensate for rainfall shortage [Mekki et al., 2006; Saha et al., 2007]. In order to elaborate decision support systems and adaptation strategies for mitigating the effects of global change, including climatic and anthropogenic forcings, there is a need for reliable estimates of land surface fluxes, especially evapotranspiration, within hilly crop fields.

Within hilly watersheds, topographical features and boundary layer conditions are very different from those observed within flat and mountainous areas, because of relief patterns, wind regimes and thermal stratification [Raupach and Finnigan, 1997]. Hill patterns and shapes influence the interception of solar radiation and the threedimensional structure of airflow in terms of pressure, direction and velocity [Raupach and Finnigan, 1997]. Such influence combines with the effect of atmospheric stability [Ross et al., 2004], as well as with land surface aerodynamic properties, including roughness through vegetation density and height [Allen, 2006]. In addition, horizontal advection may not be negligible [Poggi et al., 2008].

Experimentally, land surface fluxes have been measured in sloping conditions by using eddy covariance (EC) systems [Finnigan, 2008], mostly over mountainous areas with forests [Rannik, 1998; Geissbühler et al., 2000; Humphreys et al., 2003; Turnipseed et al., 2003] or grasslands [Hammerle et al., 2007; Hiller et al., 2008]. Due to experimental onerousness, the instrumental setups have usually involved single devices [e.g. Hammerle et al., 2007; Hiller et al., 2008; Etzold et al., 2010; Liu et al., 2012], and very rarely multiple devices that would permit the study of advection effects [Feigenwinter et al., 2008; Zeri et al., 2010]. Only a few experiments were conducted over hilly crop fields [Rana et al., 2007, 2011; Scott, 2010; Zitouna-Chebbi et al., 2012].

When using single EC devices over complex terrain, tilt correction techniques are usually applied to virtually align the sonic anemometer perpendicular to the airflow streamlines [Lee et al., 2004; Rebmann et al., 2012]. For hilly crop fields, Rana et al. [2007, 2011] and Scott [2010] applied the planar fit tilt corrections by fitting a single alignment plane over the whole time series of the considered EC dataset, thus assuming that airflow inclination does not change throughout the experiment. However, Zitouna-Chebbi et al. [2012] improved the accuracy of energy flux measurements over bare soils by discriminating between upslope and downslope winds for planar fit tilt corrections. Indeed, combined effects of wind direction and topography drove airflow inclination that was parallel to the topographical slope for upslope winds and almost horizontal for downslope winds.

For the outdoor experimental studies discussed above, the tilt corrections were applied without considering any influence of vegetation canopy on airflow inclination. However, several studies theoretically underlined this influence by using wind tunnel experiments [Finnigan and Brunet, 1995; Poggi and Katul, 2007], large eddy simulations (LES) techniques [Tamura et al., 2007; Dupont et al., 2008] and analytical modeling approaches [e.g. Finnigan and Belcher, 2004; Ross and Vosper, 2005; Patton and Katul, 2009; Harman and Finnigan, 2013]. Although limited to simple situations (sinusoidal two-dimensional hills, neutral regime, deep forest canopies), these studies permitted the identification of key drivers, and various analytical models were proposed for specific airflow regimes induced by topography-driven pressure field or vegetation canopy absorbing momentum [Poggi et al., 2008]. Finnigan and Belcher [2004] showed that deep canopies could enhance the separation region in the lee side of a hill.

In the context of obtaining reliable EC measurements of daytime energy fluxes over sloping crop fields, the current study aimed at identifying adequate tilt corrections that account for the combined effects of topography, wind direction and vegetation height on airflow inclinations. To this aim, an experiment was set up over the cycle of various crops located on the two opposite rims of a hilly watershed in a semi arid climate. The paper is structured as follows. Section 2 presents (1) the experiment, (2) the calculations of airflow inclinations, land surface energy fluxes, and local wind-oriented topography, and (3) the experimental conditions. Section 3 reports (1) the temporal changes in airflow inclinations, (2) the changes in airflow inclination as driven by the local topography and the vegetation height, and (3) the analysis of the tilt corrections of flux measurements and the energy balance closure. Section 4 and 5 discuss the main outcomes and future directions for study.

2. Materials and methods

2.1. Experimental site

The experiment was set within the agricultural Kamech watershed, located in the Cap Bon peninsula in northeastern Tunisia (36°52’40” N, 10°52’40” E). A description of the Kamech watershed can be found in Mekki et al. [2006]. This watershed belongs to the long-term environmental research observatory OMERE (a French acronym for the Mediterranean Observatory of Water and the Rural Environment). Within rural watersheds, OMERE studies the impacts of anthropogenic forcing and climate change on hydrology, erosion, and water quality (http://www.umr-lisah.fr/omere).

The El Gameh wadi crosses the 2.45 km^2 Kamech watershed from the northeast to the southwest. The watershed topography is entirely V-shaped from its middle to the outlet (Figure 1). The slopes are irregular, especially on the southern rim, which has natural embankments induced by sandstone hogbacks. The altitude ranges between 94 m and 194 m. The slopes range between 0% and 30%. The soils have sandy-loam textures, with depths ranging from zero to two meters according to the location within the watershed and to the local topography. These swelling soils exhibit shrinkage cracks under dry conditions during the summer [Raclot and Albergel, 2006].

[Figure 1 about here]

The regional climate is sub-humid with annual values of 600 mm and 1500 mm for precipitation and the Penman-Monteith reference crop evapotranspiration, respectively. The main crops are rainfed. They include winter cereals (durum and bread wheat, barley, oat, triticale) and legumes (chickpeas, favabeans), which can be either harvested or grazed. The steepest parts of the watershed are covered by natural vegetation and used as rangeland for livestock.

2.2. Measurement locations and experimental calendar

The flux measurements were conducted during several months over field A, B and C (Figure 1). In 2004 and 2006, a flux station was installed in field A, located on the northern rim of the watershed. Field A had an area of 1.1 ha with a homogeneous slope of 5° facing south-southeast. This field's northern (and upper) limit was close to the rim top, which forms the watershed edge. In 2005, a flux station was installed in field B, located close to field A. This field had an area of 1.6 ha, and its topographical and pedological conditions were very similar to those of field A. To assess any possible effect of slope orientation on energy fluxes, a second flux station was installed in 2006 in field C, located on the southern rim of the watershed and facing northwest. Field C had an area of 2.2 ha and an irregular topography. The averaged slope around its center was approximately 8°. The field's southern (and upper) limit was close to a plateau, located in the middle of the rim. Its northern (and lower) limit had a natural embankment induced by a sandstone hogback. The terrain along-wind cross-sections around flux stations A and C are given in Figure 6 of Zitouna-Chebbi et al. [2012], and the local topography around flux station B was similar to that around flux station A.

The flux measurements were collected under conditions of bare soil and vegetation cover, which are detailed in Table 1. In 2004, field A was a wheat crop, and the measurements were collected from March 30 to November 4. In 2006, field A was a favabean crop, and the measurements were collected from March 3 to July 28. In 2005, field B was an oat crop, and the measurements were collected from January 18 to June

20. In 2006, field C was a rangeland, and the measurements were collected from April 13 to July 27. The corresponding four datasets were labeled A04, A06, B05 and C06, where the letter represents the field, and the two digits represent the year.

[Table 1 about here]

2.3. Calculations of land surface energy fluxes in sloping conditions

2.3.1. Flux station measurements

The sensible and latent heat fluxes, soil heat flux and net radiation were measured with similar flux stations at fields A, B and C. The instruments for each flux station are listed in Table 2. The sonic anemometers and krypton hygrometers collected raw data at a 10 Hz frequency. The raw data were stored in the CR23X datalogger, and downloaded every minute to a laptop through the RS232 serial port. The flux measurement stations for dataset A04 and C06 were new. The same flux measurement station was used for dataset A04, B05 and A06. For dataset B05 and A06, the krypton hygrometer did not operate, because of instrumental degradation induced by the alternation between dry and wet periods.

[Table 2 about here]

For each flux station, the three soil heat flux sensors were distributed two meters away from the station, and were buried between 20 and 50 mm below the soil surface. The net radiometers were installed 1.5 m above the ground. The sonic anemometers, the krypton hygrometers, and the air temperature and humidity probes were installed at the same height above the ground during each period of data acquisition: 1.96 m, 1.78 m, 2.05 m and 2.02 m for dataset A04, A06, B05 and C06, respectively. It was a posteriori verified that these measurement heights were appropriate, since they were located within the inertial sublayer (Section 2.5.2).

The sonic anemometers were vertically setup and oriented relative to North. The net radiometers were horizontally setup. Instrument setups were carefully checked during the experiment, as described in Zitouna-Chebbi et al. [2012]. The latter investigated the accuracy on sonic anemometer alignments according to the experimental protocol and to the analysis of airflow inclination data. The proposed accuracy was better than 2° absolute.

Batteries and solar panels powered the data acquisition systems. Because of the high power consumption of the laptop computers, several battery failures occurred, and the 10 Hz data acquisitions were not continuous [Zitouna-Chebbi et al., 2012]. After gap filtering, the numbers of 30-minute intervals with 10 Hz data acquisition were 550, 1609, 975 and 1286 for datasets A04, A06, B05 and C06, respectively. This corresponded to 10%, 48%, 29% and 52% of daytime observations, evenly distributed throughout the experimental periods.

2.3.2. Calculating airflow inclinations according to wind direction and vegetation height

The angles for characterizing the airflow inclinations were calculated from the sonic anemometer data. The calculations were conducted using the planar fit (PF) method [Wilczak et al., 2001] implemented within the ECPACK library version 2.5.22 [van Dijk et al., 2004]. The PF method was chosen since it overcomes the drawbacks of concurrent solutions [Rebmann et al., 2012].

The sonic anemometers measured wind speed in three perpendicular directions (labeled *u* and *v* in the horizontal plane and *w* in the vertical plane). In order to virtually align them perpendicularly to the airflow streamlines, the PF method determined the required rotations as defined by three angles: the yaw angle, which was a rotation around the vertical axis that aligned *u* with the mean wind direction; the pitch angle, which was a rotation around the horizontal axis perpendicular to the wind direction that nullifies the *w* mean value; and the roll angle, which was a rotation around the horizontal axis parallel to the wind direction. Assuming the airflow streamlines were included in a plane, the latter was fitted to the 10-Hz wind speed components collected over a given time interval.

A single plane might not adequately represent the airflow inclinations for different wind directions and vegetation heights. First, local topography induced anisotropic airflows, and the tilt angles (pitch and roll) were supposed to depend upon the wind direction (yaw angle). Second, changes in vegetation height were supposed to influence airflow inclination, because of the cross influences of topography and canopy. Therefore, the 10-Hz EC data were gathered within intervals of wind direction (or wind sectors) and intervals of vegetation height *hv*. The numbers of wind sectors and vegetation height intervals to be considered were determined according to analysis results for wind data (Section 2.5.1) and vegetation data (Section 2.5.2).

For each dataset (A04, A06, B05 and C06), two calculations were made to ensure that the PF angles were not sensitive to the time interval over which they were estimated. The daily plane calculation consisted of fitting one plane for each wind sector and each day (or a portion of day when the wind direction changed). The single plane calculation consisted of fitting a unique plane over all the data belonging to a given wind sector and to a given *hv* interval (several days for a given wind sector and a given *hv* interval). Similarly to Zitouna-Chebbi et al. [2012], it was a posteriori verified that these two methods provided similar airflow inclinations (Section 3.2).

For any plane inclination provided by the PF method, it was possible to calculate the airflow inclination for any observed wind direction (yaw angle). The resulting tilt angles will be referred to as PF pitch and roll angles hereafter. For daily plane calculation, we determined the PF pitch and roll angles for the mean yaw angle of each wind sector. For single plane calculation, we determined the PF pitch and roll angles for any 1° step yaw angle value within the considered wind sector.

Uncertainties on airflow inclinations resulted from both the 2° absolute error on EC device alignments (Section 2.3.1) and the errors in planar fit calculations. Both error sources were not considered as critical. First, the daily plane and single plane calculations provided similar airflow inclinations, as shown in Zitouna-Chebbi et al. [2012] and as verified a posteriori in Section 3.2. Second, airflow inclinations were not analyzed in absolute, but in relative through (1) differences in airflow inclinations and topographical slopes, (2) differences in airflow inclinations for upslope and downslope winds, and (3) differences in airflow inclinations for various vegetation heights.

2.3.3. Calculating convective fluxes according to airflow inclination

The convective fluxes (friction velocity u_*, sensible heat flux H and latent heat flux λE) were calculated from the sonic anemometer and the krypton hygrometer data, over 30-minute intervals, by using the ECPACK library version 2.5.22 [van Dijk et al., 2004].

Most of the instrumental corrections proposed in the ECPACK library were applied. These corrections addressed (1) the calibration drift of the krypton hygrometer;

(2) the linear trends over the 30-minute intervals; (3) the sonic anemometer temperature for humidity; (4) the hygrometer response for oxygen sensitivity; (5) the mean vertical velocity (Webb term); (6) the correction for the frequency response and path averaging; and (7) the tilt corrections for airflow inclination. When correcting the convective fluxes for airflow inclination (item 7), we considered the PF pitch and roll angles derived from the daily plane calculation (Section 2.3.2).

A side-by-side comparison of the EC measurement devices was conducted during one month within field A. This comparison aimed at ensuring it was possible to compare the measurements collected within the three fields. Instrumental differences on sensible and latent heat flux (e.g. root mean square difference of 20 W m^{-2}) were within the widely accepted accuracies for the EC data [Foken, 2008; Xu et al., 2013].

The quality control of the 30-minute flux data was performed using two standard tests that are routinely employed over flat and sloping terrains, i.e. the Steady State test and Integral Turbulence Characteristics test. These tests permitted to ensure that the theoretical requirements for the EC measurements were fulfilled [Hiller et al., 2008]. Following Zitouna-Chebbi et al. [2012], we kept the high and good quality data as defined by Foken et al. [2004] and Rebmann et al. [2005]. For bare soil conditions (respectively vegetation cover conditions), the selection rate was 98% and 69% (respectively 95% and 85%) for the sensible and latent heat flux data.

The footprint of each 30-minute flux data was estimated as the ellipsoid from which 90% of the flux originated, by using the approach of Horst and Weil (1992). Each footprint was next superimposed on the digital map of the field boundaries, to quantify each flux contribution from target field (Mauder et al., 2013). Median values for the flux contribution from target field were 67%, 66%, 78% and 80% for datasets A04, A06, B05 and C06, respectively. We did not observe notable differences between northwest and south winds. As compared to bare soil conditions (Zitouna-Chebbi et al., 2012), the flux contributions from target fields were larger for vegetation cover conditions, by 15% relative. These larger contributions were explained by decreasing footprints as vegetation grew. Overall, the flux contributions from target fields were about 75%, whereas the field surveys indicated, in most cases, similar conditions for vegetation canopy cover and soil water status within the target and surrounding fields.

2.3.4. Calculations of net radiation and soil heat flux

The calculations of net radiation *Rn* and soil heat flux *G* are detailed in Zitouna-Chebbi et al. [2012].

The *Rn* measurements were corrected for the effects of slope following the procedure proposed by Holst et al. [2005] that relied on solar irradiance and topographical data. Solar irradiance data were derived from measurements collected at the meteorological station located near the watershed outlet (see label M on Figure 1 and Section 2.5.1). Topographical data were derived from a four-meter spatial resolution digital elevation model (DEM) obtained by photogrammetry with a stereo pair of panchromatic Ikonos images [Raclot and Albergel, 2006]. The magnitude of the correction on *Rn* was 50 W m^{-2} on average. A side-by-side comparison of NR-lite net radiometers was conducted during one month within the same field. We observed instrumental differences within the instrumental accuracies, i.e. root mean square difference of 20 W m^{-2}.

Soil heat flux *G* was estimated by averaging the measurements collected by the three soil heat flux sensors distributed around each flux station. No correction was applied for the heat storage between the surface and the sensors, since existing solutions are questionable when considering swelling soils. This was not considered to be a critical issue. Indeed, the resulting error had the same magnitude (20-50 W m^{-2}) as the measurement uncertainty resulting from the instrumental errors or the spatial variability [Olioso et al., 2002; Shao et al., 2008; Leuning et al., 2012].

2.4. Calculation of the wind oriented topography

The characterization of the local topography in the vicinity of each flux station is detailed in Zitouna-Chebbi et al. [2012]. It relied on the data derived from the four-meter spatial resolution DEM (Section 2.3.4).

First, we defined a rectangle centered on the flux station and oriented along each wind direction (yaw angle). The length and width of the rectangle were derived from the length and width of the ellipsoidal footprints. For the sake of simplicity, we considered the nominal values set by Zitouna-Chebbi et al. [2012] under bare soil conditions, which corresponded to twice the median values of the footprint dimensions (360 m for the length and 120 m for the width). We considered this rectangle size to account for the influence of the upstream / downstream topography on the airflow inclination.

The rectangles were calculated for 1° step yaw angle values between 0 and 360°. For each rectangle, a topographical plane was fitted against the corresponding DEM altitude data. The topographical plane equation was next used to define the wind-oriented topography by calculating an along-wind terrain slope geometrically similar to the PF pitch angle (Section 2.3.2) that will be referred to as terrain pitch angle hereafter.

It was understood that changes in vegetation height might induce changes in the terrain area that influenced airflow inclination. Therefore, the sensitivity of the terrain pitch angle estimates to the rectangle length was evaluated by using two extreme values for the latter. The first length was 50 m, corresponding to topographical variations at the field scale. The second length was 300 m, corresponding to topographical variations at the hillslope scale. The resulting variation in terrain pitch angle was small, by 0.2° on average.

2.5. Characterization of the experimental conditions.

2.5.1. Micrometeorological conditions

We characterized the micrometeorological conditions throughout the several months of experiment. We considered the data collected on the four locations within the watershed (Figure 1): two locations on the northern rim (EC data on field A in 2004 and 2006, and on field B in 2005), one location on the southern rim (EC data on field C in 2006) and one location close to the outlet (meteorological station in 2004, 2005 and 2006). Details about the meteorological station are given in Zitouna-Chebbi et al. [2012].

Wind speed data, 4 m s^{-1} on average, were twice the worldwide mean values of the Food and Agricultural Organization over lands at 2 m height [Allen et al., 1998]. Under bare soil conditions, wind speed did not vary by more than 1 m s^{-1} within the study area. Wind direction data did not depict any diurnal cycle, and they provide similar distributions over the different locations within the watershed. We noted two dominant sectors, as illustrated in Figure 4 in Zitouna-Chebbi et al. [2012]. The first sector corresponded to winds coming from directions between southwest (220°) and east-northeast (70°) directions (clockwise degrees, North is 0°), hereafter referred to as northwest winds. The second sector corresponded to winds coming from the other directions, hereafter referred to as south winds. As the two dominant wind directions were almost perpendicular to the valley axis, the northwest winds corresponded to downslope winds over the northern rim (field A and B) and to upslope winds over the southern rim (field C). The converse applied for the south winds.

Micrometeorological conditions were analyzed using the atmospheric stability parameter $\zeta = (z-d)/ L_{MO}$, where z is measurement height, d is displacement height and L_{MO} is Monin-Obukhov length. ζ was always negative, with notably few values less than -0.1. When considering each of the dataset A04, A06, B05 and C06 as a whole, ζ median values ranged between -0.052 and -0.018. ζ values were twice to four times more negative for bare soil conditions (between -0.056 and -0.040) as compared to vegetation cover conditions (between -0.029 and -0.014). We did not observe notable differences between northwest and south winds.

Overall, the micrometeorological measurements indicated that the wind regime was externally driven and that the stability regime corresponded to forced convection. First, the site experienced large wind speed values. Second, the wind direction did not depend upon the local topography and did not depict any diurnal circulation (i.e. valley breezes). Third, bare soil conditions mostly corresponded to low atmospheric instability, and vegetation cover conditions mostly corresponded to neutral conditions.

2.5.2. Vegetation conditions

We characterized the vegetation conditions throughout the growth cycles for crops (field A in 2004 and 2006, field B in 2005) and rangeland (field C in 2006). For dataset A04 and B05, cereal crops corresponded to homogeneous canopies. For dataset A06 and C06, favabean crop and pasture corresponded to heterogeneous canopies. The favabean crop was row structured and thus partially covering. The pasture was a randomly sparse canopy.

Vegetation height *hv* was measured using a tape measure. For crops (respectively rangeland), a set of 30 (respectively 100) samples per field was considered. Frequency of measurement collection ranged between two and four weeks, in accordance to the vegetation growth observed within the field. A randomly distributed spatial sampling was designed in accordance to each field heterogeneity. For a given day of data collection and a given field, *hv* was estimated by calculating over the samples both the averaged value of the measurements and the corresponding standard deviation. We next linearly interpolated the averaged values to obtain daily values between days of data collection.

Figure 2 displays the temporal evolution of vegetation height *hv* for the datasets A04, A06, B05 and C06. Maximum values for *hv* are indicated in Table 1. Two types of temporal evolution were noted. The first type was related to covering vegetation such as the cereal crops for dataset A04 and B05. It was characterized by a growth period, followed by a maturity plateau and next a steep decrease at harvest with vegetation cut. The second type was related to sparse vegetation such as the favabean crop for dataset A06 and the pasture for dataset C06. It differed from the first type after the maturity plateau. For dataset A06, the difference was the absence of vegetation cut (only beans were harvested). Thus, the senescence period induced a slight decrease of vegetation height only, which next combined with the emergence of natural vegetation after rainfalls. For dataset C06, the difference was the occurrence of grazing events, although the latter did not impact the temporal dynamics of vegetation height at the field scale, because of spatial heterogeneities.

[Figure 2 about here]

The hv dataset further permitted to verify the consistency of the experimental setup. The EC devices were setup around 2 m above the ground (Section 2.3.1), which induced a measurement height that was at least twice larger than the vegetation height hv. Therefore, the measurement height was located within the inertial sublayer above the roughness sublayer, the latter extending from the ground up to 1.43 x hv [Pattey et al., 2006]. This applied to our experimental conditions (neutral or slightly unstable conditions, as explained in Section 2.5.1), but might not be valid during nighttime and / or under stable or very unstable conditions.

The hv dataset was further used to analyze the airflow inclination in relation to the local topography (Section 3.2). For this, three intervals of vegetation height were considered (in meters): $hv \in [0-0.4[$; $hv \in [0.4 - 0.6[$; $hv \in [0.6-1[$. Finally, vegetation cuts were of interest when seeking any influence of canopy height on airflow inclination, since such temporal discontinuities were expected to induce sharp changes.

3. Results

We first address the temporal evolutions of the airflow inclinations as captured by the EC devices, in relation to changes in vegetation height (Section 3.1). We next analyze the influence of both local topography and vegetation height on airflow inclinations (Section 3.2). For this, we compared the airflow inclination against the terrain slope by considering different intervals of vegetation height. Once the EC data are corrected for airflow inclination by discriminating upslope / downslope winds and levels of vegetation height, we finally deal with the reliability of the corrected EC data by analyzing the energy balance closure (Section 3.3).

We focus on daytime measurements, since nighttime values of sensible and latent heat fluxes are small at the daily timescale. For airflow inclination analysis, the terrain pitch angle and PF pitch angle had the same sign definition. Positive values of the terrain pitch angle corresponded to upslope winds, and positive values of the PF pitch angle corresponded to upward airflows. Negative values of the terrain pitch angle corresponded to downslope winds, and negative values of the PF pitch angle corresponded to downward airflows.

3.1. Temporal evolutions of airflow inclinations in relation to vegetation height

Figure 3 displays an example of the temporal evolutions of the vegetation height and of the PF pitch angle for upslope and downslope winds. These typical evolutions were obtained with the longest-lasting B05 dataset that included vegetation cut and that depicted the largest temporal changes in vegetation height (Figure 2). As vegetation height increased from 0.15 to 1 m throughout the vegetation growth period, the PF pitch angle decreased from 0 to -5° for downslope winds; and from 5.5 to 3° for upslope winds. The changes in PF pitch angle were twice larger for downslope winds (5°) than for upslope winds (2.5°). Immediately after vegetation cut, both the vegetation height and the PF pitch angle returned to their initial values at the beginning of the growing period.

[Figure 3 about here]

The behaviors we observed with the A04 dataset (data not shown) were very similar to those reported when analyzing the B05 dataset. On the one hand, the two datasets depicted sharp changes in PF pitch angle after vegetation cut, for both upslope and downslope winds. On the other hand, the two datasets depicted larger changes in PF pitch angle for downslope winds than for upslope winds. Different behaviors were noted with the A06 and C06 datasets (data not shown): lower variations of PF pitch angle throughout the experiment were related to slighter evolutions of vegetation height, as previously noted (Figure 2).

3.2. Airflow inclinations as driven by topography and vegetation height

For each dataset (A04, A06, B05 and C06), the planar fit (PF) angle calculation was twofold (Section 2.3.2). The daily plane calculation yielded between more than 10 and less than 20 daily planes, according to the number of 30-minute intervals of 10-Hz data collected (Section 2.3.1). The single plane calculation yielded two planes corresponding to the northwest and south wind sectors for each of the three *hv* intervals.

Figure 4 compares the terrain slopes and the airflow inclinations, as a function of wind direction, for each of the four datasets (A04, A06, B05 and C06). The continuous lines represent the terrain pitch angle along the wind direction, as derived from the DEM data. The airflow inclinations are represented by the PF pitch angles that are derived either from the daily plane calculation (symbols) or from the single plane calculations (dashed or dotted lines according to vegetation height *hv*).

[Figure 4 about here]

Regardless of dataset (A04, B05, A06 and C06), wind sector (northwest and south) and *hv* interval, PF pitch angles given by the daily plane calculation and the single plane calculation were in close agreement. Changes in vegetation height induced changes in pitch angle, as indicated by the splitting of each dataset into the three *hv* intervals. Further, positive values for PF pitch angle indicate that upward airflows corresponded to upslope winds, and negative values for pitch angle indicate that downward airflows corresponded to downslope winds.

Three specific behaviors were observed through the analysis of the PF pitch angle as a function of vegetation height and of upslope / downslope winds.

- When considering upslope winds with bare soil and low vegetation heights ($hv < 0.4$ m) for the datasets A04, B05 and A06, the PF pitch angles were close to the terrain pitch angles, which indicated that the airflow inclinations were close to the terrain slope. Increase in vegetation height ($hv > 0.6$ m) induced a slight decrease in PF pitch angle, between 1 and 2°, which indicated that the airflow inclination tended to be less tilted than the terrain slope.
- When considering downslope winds under conditions of bare soil and low vegetation heights ($hv < 0.4$ m) for the datasets A04, B05 and A06, the PF pitch angle was larger than the terrain pitch angle, of about 3 to 5°. In this case, the PF pitch angle was closer to nil, and thus the airflow inclination was close to the horizontal plane. Increase in vegetation height ($hv > 0.6$ m) induced a decrease in PF pitch angle of about 4°. Then, the latter almost equaled the terrain pitch angle, which indicated that the airflow inclination came closer to the terrain slope.
- When considering dataset C06 that corresponded to conditions of low vegetation height only ($hv < 0.4$ m), there was a good agreement between terrain pitch angle and PF pitch angle for both upslope and downslope winds, which indicated that airflow inclination almost followed the terrain slope.

Overall, the following trends can be reported. For upslope winds, airflow inclination was close to the terrain slope under conditions of bare soil and low vegetation height, and it was less tilted as vegetation height increased. The converse was observed for downslope winds: airflow inclination was only slightly tilted under conditions of bare soil and low vegetation height, and it was more tilted as vegetation height increased, thus coming closer to the terrain slope. As compared to upslope winds, we observed larger changes in airflow inclination for downslope winds, when vegetation height increased. The behaviors reported here were systematically observed for dataset A04, B05 and A06. For dataset C06 that corresponded to low vegetation height, we noted a systematic agreement between airflow inclination and terrain slope, regardless of upslope and downslope winds.

We next attempted to isolate the relation between vegetation height and airflow inclination, by characterizing the shifted pitch angle (defined as the difference between PF pitch angle and terrain pitch angle) as a function of the vegetation height *hv* (Figure 5). or this, we considered the dataset B05 that spread over the vegetation growth cycle, thus capturing a large dynamics of vegetation height. Figure 5 shows that the shifted pitch angle was strongly related to *hv*, with a larger dynamics for downslope winds (changes of about 4.5°) as compared to upslope winds (changes of about 1.5°). The relation between shifted pitch angle and *hv* appeared to be linear, with coefficients of determination R^2 ranging from 0.68 for upslope winds to 0.85 for downslope winds. When considering the other datasets (data not shown), the trends were less pronounced because of lower vegetation dynamics. Nevertheless, the linear regressions obtained for dataset B05 where similar to those obtained for dataset A04, where the latter spread over the senescence period and the harvest time only.

[Figure 5 about here]

3.3. Correction of convective fluxes and energy balance closure

The EC measurements of convective fluxes were corrected for airflow inclination. The tilt correction was conducted by using the PF pitch angles derived from the daily plane calculation, thus discriminating between upslope and downslope winds, and discriminating between levels of vegetation height (Section 2.3.3). For upslope winds (respectively downslope winds), the tilt correction increased (respectively decreased) H and λE by 37% (respectively 17%) on average over the datasets. The magnitude of the tilt correction was larger on average as the airflow inclination was larger. For field A with upslope winds, the tilt correction increased H and λE by 30%, and by 40% on field C with steeper slopes. For field B with downslope winds, the magnitude of the tilt correction was lower with less tilted airflows over low vegetation ($hv < 0.4$ m), by 20% for H, as compared to more tilted airflows over tall vegetation ($hv > 0.6$ m).

We analyzed the energy balance closure by comparing the convective fluxes CF ($CF = H + \lambda E$) against the available energy $AE = Rn - G$. Although the usefulness of such analysis as a quality test may be debatable [Lee et al., 2004], it was considered as an interesting comparison of independent measurements. The data to be compared were those calculated over the 30-minute intervals (Section 2.3.3 and Section 2.3.4).

Since no latent heat flux data were collected for the datasets A06 and B05, because of the krypton hygrometer inoperability, the energy balance closure could be analyzed for datasets A04 and C06 only. The number of available observations for assessing the energy balance closure was constrained by the availability of the four components of the energy balance (net radiation Rn, soil heat flux G, sensible H and latent λE heat fluxes) and by the quality control filtering (Section 2.3.3).

The analysis of energy balance closure was conducted by discriminating between upslope and downslope winds and by discriminating between bare soil and vegetation cover. Following Zitouna-Chebbi et al. [2012] who addressed energy balance closure for bare soil conditions, we considered here the results obtained for both bare soil and vegetation cover conditions (Figure 6). The corresponding statistical indicators are given in Table 3.

[Figure 6 about here]

[Table 3 about here]

The energy balance closure, as expressed through the energy balance ratio *EBRAT* = *CF* / *AE*, ranged from 83% to 94%, with the exception of the downslope winds for dataset C06 that corresponds to 73% for both bare soil or vegetation cover. Also, *CF* systematically underestimated *AE* for large values.

The energy balance closure was similar if considering bare soil or vegetation cover conditions, with the following statistical indicators (defined in Table 3 caption): energy balance residual *EBRES* ranged from 20 to 95 W m^{-2}, root mean square difference *RMSD* ranged from 45 W m^{-2} to 110 W m^{-2}, coefficient of determination R^2 ranged from 0.88 to 0.95, slope and offset values for the linear regression from *CF* to *AE* ranged from 0.65 to 0.8 and from 20 to 46 W m^{-2}, respectively.

We finally analyzed the energy balance closure as a function of the upslope and downslope winds. For dataset A04, the statistical indicators were slightly better with downslope winds as compared to upslope winds (Table 3): *RMSD* was 20 W m^{-2} lower, *EBRAT* was 10% larger, *EBRES* was twice lower, and the slope value for the linear regression from *CF* to *AE* was 10% larger. For dataset C06, conversely to A04, the statistical indicators were better for the upslope winds as compared to the downslope winds (Table 3): *RMSD* was 60 W m^{-2} lower, *EBRAT* was 20% larger, *EBRES* was four to five times lower, and the slope value for the linear regression from *CF* to *AE* was 15% larger.

4. Discussion

The trends we observed when analyzing the temporal evolutions of airflow inclination as captured by the EC based pitch angles were consistent with the dynamics of vegetation height. On the one hand, sharp changes in PF pitch angles systematically occurred after harvest for datasets A04 and B05, where vegetation cut reset airflow inclination to its initial value at the beginning of the crop growth cycle. On the other hand, lower variations of PF pitch angle throughout the experiment for datasets A06 and C06 were ascribed to the slighter evolutions of vegetation height: the harvest was restricted to bean collection for dataset A06, and the vegetation dynamics of the pasture resulted in slight changes for dataset C06. These observations suggested that changes in airflow inclinations were strongly linked to changes in vegetation height. We did not ascribe changes in airflow inclinations to changes in atmospheric stability conditions, since the latter depicted a narrow range, between neutral and very low instability regimes.

When analyzing airflow inclination over bare soils, upslope winds induced behaviors similar to those observed under flat conditions, since the streamlines followed the local topography. A different behavior was observed for downslope winds with datasets A04, A06 and B05. This was consistent with theoretical works on streamline dilatation in relation to the non-separated sheltering effect [Belcher et al., 1993], where fields A and B were located in the lee of the hilltop. Further, momentum absorption by the canopy foliage explained changes in airflow inclinations when vegetation height increased, from the terrain slope to less tilted planes under upslope winds, and from nearly the horizontal plane to the terrain slope under downslope winds.

Two types of airflow regime were identified according to the classification proposed by Poggi et al. [2008], which is based on the ratio of vegetation height hv to the canopy adjustment length scale Lc (deep or shallow canopies), and on the ratio of the along-wind hill length Lh to the hill height Hh (narrow or long hills). When considering the two watershed rims and the two dominant wind directions, Lh (respectively Hh) ranged between 200 and 400 m (respectively 40 and 60 m). Following the aforementioned classification, the airflow regimes we observed corresponded to regime IV (shallow canopy) at the beginning of the growth cycle ($Lh / (2\ Lc)$ around 3.5 and hv / Lc around 6.10^{-4}), and to Regime I (deep canopy) or IV (shallow canopy) at the end of the growth cycle ($Lh / (2\ Lc)$ between 60 and 220 and hv / Lc between 0.1 and 0.7). Following Poggi et al. [2008], we can conclude that (1) airflow above the canopy was primarily driven by the topography, (2) the changes in airflow inclination when vegetation grew could be ascribed to increase in momentum absorption by the canopy foliage when the latter became thicker, and (3) the advection remained small.

When applying the tilt correction in the calculation of H and λE, it was necessary to discriminate not only between upslope and downslope winds but also between vegetation heights. As more tilted airflows induced larger corrections, fitting a single plane for both upslope and downslope winds and regardless of vegetation height would induce intermediate values for PF pitch angle, and therefore would provide wrong tilt corrections for H and λE.

The results obtained for energy balance closure also emphasize the relevance of discriminating upslope / downslope winds and intervals of vegetation height, when applying the tilt correction on convective fluxes. For upward airflows, the correction increased the convective fluxes by 30% relative and thus improved by the same magnitude the energy balance closure that was characterized by an underestimation of available energy. For downward airflows on field A, the correction decreased the convective fluxes, thus making their sum lower than available energy. The unique case for which we did not observe any improvement is related to downward airflows on field C, where the tilt correction increased the underestimation of available energy.

No correction was applied on soil heat flux measurements for soil heat storage between the surface and the sensors, since existing solutions are questionable when considering swelling soils. Also, canopy heat storage was not taken into account, since it is both difficult to estimate and usually disregarded for agricultural crops. Neglecting both canopy and soil heat storage resulted in overestimating available energy and thus increasing energy balance disclosure. On average, including canopy and soil heat storage would decrease available energy by 1 - 3% and 2 - 5% relative, respectively (Wang et al., 2010), and thus would raise energy balance ratio (EBRAT) between 88% and 99%, especially at mid-day. This EBRAT increase indicates the effectiveness of the correction method we proposed.

Overall, and regardless of the considered case (field, year, wind direction, bare soil or vegetation cover), the statistical indicators for energy balance closure after tilt corrections were comparable to those reported in previous studies [Wilson et al., 2002; Hammerle et al., 2007; Foken, 2008; Hendricks Franssen et al., 2010; Wang et al., 2010; Malone et al., 2014] that considered different topographies (flat and mountainous topographies) and different vegetation cover conditions (bare soils and various canopies).

Several explanations can be proposed for the different results we observed for field C, including (1) the complex topography of the southern rim, (2) the differences in hill shapes and sizes within the southern rim, or (3) the locations of the EC flux stations within the hillslopes for downslope winds: fields A and B were located in the lee of the northern rim top and close to it, whereas field C was located further from the southern rim top. Besides, Finnigan and Belcher [2004] also reported asymmetry in the flow between upslope and downslope winds, as observed on field A but not on field C. However, any comparison with outcomes from modeling studies should be carefully conducted. On the one hand, these modeling studies addressed simple situation such as single or periodic two-dimensional hills. On the other hand, the experimental study we report here addressed complex hilly structures with various hill shapes.

5. Concluding remarks

Main outcomes from the current study are twofold. First, airflow inclination was strongly influenced by the combined effects of wind direction, topography and vegetation height. Changes in airflow inclination were observed for upward and downward airflows, and for different levels of vegetation height. Second, when applying planar fit tilt corrections on EC measurements, it was necessary to discriminate not only between upward and downward airflows, but also between vegetation height intervals. This discrimination permitted to improve the EC measurements and thus to obtain reliable estimates of daytime energy fluxes over hilly crop fields.

The experimental observations we reported here can be ascribed to specific airflow regimes previously reported in theoretical studies, such as streamline dilatation / contraction and non-separated sheltering effect, momentum absorption by the canopy foliage, and relative location within the hillslope. This consistency between experimental and theoretical outcomes increases our confidence in the measurements we discussed here.

Topography and wind direction can vary significantly from one place to another within any hilly watershed, with changing influences on airflow inclination and planar fit tilt corrections for flux measurements. Therefore, it is necessary to account for possible influence of wind direction and vegetation height on airflow inclination, when applying planar fit tilt corrections over hilly terrains.

The experimental observations we reported here were focused on the observation of land surface energy and mass (water vapor) fluxes. However, it is most likely that these observations do also apply when observing other mass fluxes such as carbon dioxide, methane or volatile organic compounds. We therefore recommend to conduct such investigations.

Finally, our experimental observations cast into doubt the relevance of using common modeling tools within hilly crop fields, since these tools were developed for flat conditions. As mentioned by Finnigan and Belcher [2004], canopy roughness length is likely to change with accelerating and decelerating flow over hills, with consequences on aerodynamic resistance. Investigating such questions will enable the expansion of the recent modeling works by Rana et al. [2007], and should imply new formulations for the operational FAO-56 method proposed by Allen et al. [1998].

Acknowledgments

The data used in this study are available according to the data policy of the Environmental Research Observatory OMERE (http://www.umr-lisah.fr/omere). Financial support for this study was provided by (1) the French Institute of Research for Development (IRD) through the Department for Support and Training; (2) the European Union (Fifth Framework Program) through the IRRIMED project (contract ICA3-2002-10080); (3) the Agropolis Foundation (Thematic Network of Advanced Research "Montpellier Agronomy and Sustainable Development") through the "Land surface atmosphere exchanges within hilly watersheds" project (contract 0901-013); (4) the MISTRALS / SICMED program; and (5) the French National Research Agency (ANR) TRANSMED program through the ALMIRA project (contract ANR-12-TMED-0003). We wish to thank the JGR - Atmospheres Editorial and Review Board for the fruitful comments that helped us to improve the paper.

References

Abedinpour, M., A. Sarangi, T. Rajput, M. Singh, H. Pathak, and T. Ahmad (2012), Performance evaluation of AquaCrop model for maize crop in a semi-arid environment, Agric. Water Manage., 110, 55-66, doi:10.1016/j.agwat.2012.04.001.

Allen, R. G., L. S. Pereira, D. Raes, and M. Smith (1998), Crop evapotranspiration: Guidelines for computing crop water requirements, *FAO Irrigation and Drainage Paper No. 56*. Rome, Italy: FAO.

Allen, R. G., L. S. Pereira, T. A. Howell, and M. E. Jensen (2011), Evapotranspiration information reporting: I. Factors governing measurement accuracy, Agric. Water Manage., 98, 899-920, doi:10.1016/j.agwat.2010.12.015.

Allen, T. (2006), Flow over hills with variable roughness, Boundary Layer Meteorol., 121(3), 475-490, doi:10.1007/s10546-006-9086-0.

Belcher, S., T. Newley, J. Hunt (1993), The drag on an undulating surface induced by the flow of a turbulent boundary layer, J. Fluid Mech., 249, 557-596, doi: 10.1017/S0022112093001296.

Boone, A., et al. (2009), The AMMA Land Surface Model Intercomparison Project (ALMIP), Bull. Am. Meteorol. Soc., 90(12), 1865-1880, doi:10.1175/2009BAMS2786.1.

Cai, X., Z.-L. Yang, C. H. David, G.-Y. Niu, and M. Rodell (2014), Hydrological evaluation of the Noah-MP land surface model for the Mississippi River Basin, J. Geophys. Res. Atmos., 119, 23-38, doi:10.1002/2013JD020792.

Chen, J., B. Chen, T. A. Black, J. L. Innes, G. Wang, G. Kiely, T. Hirano, and G. Wohlfahrt (2013), Comparison of terrestrial evapotranspiration estimates using the mass transfer and Penman-Monteith equations in land surface models, J. Geophys. Res. Biogeosci., 118, 1715-1731, doi:10.1002/2013JG002446.

Courault, D., B. Seguin, and A. Olioso (2005), Review on estimation of evapotranspiration from remote sensing data: From empirical to numerical modeling approaches, Irrig. Drain. Syst., 19(3-4), 223–249, doi:10.1007/s10795-005-5186-0.

Dupont, S., Y. Brunet, and J. J. Finnigan (2008), Large-eddy simulation of turbulent flow over a forested hill: Validation and coherent structure identification, Q. J. R. Meteorol. Soc., 134, 1911-1929, doi:10.1002/qj.328.

Etzold, S., N. Buchmann, and W. Eugster (2010), Contribution of advection to the carbon budget measured by eddy covariance at a steep mountain slope forest in Switzerland, Biogeosciences 7(8), 2461-2475, doi:10.5194/bg-7-2461-2010.

Feigenwinter, C., et al. (2008), Comparison of horizontal and vertical advective CO2 fluxes at three forest sites, Agric. For. Meteorol., 148(1), 12-24, doi:10.1016/j.agrformet.2007.08.013.

Finnigan, J. (2008), An introduction to flux measurements in difficult conditions, Ecol. Appl., 18(6), 1340-1350, doi:10.1890/07-2105.1.

Finnigan, J. J., and S. E. Belcher (2004), Flow over a hill covered with a plant canopy, Q. J. R. Meteorol. Soc., 130(596), 1-29,doi: 10.1256/qj.02.177.

Finnigan, J. J., and Y. Brunet (1995), Turbulent airflow in forests on flat and hilly terrain, *Wind and Trees*, M. P. Coutts, J. Grace, 3-39, Cambridge Univ Press, New York.

Foken, T. (2008), The energy balance closure problem: An overview, Ecol. Appl., 18(6), 1351-1367, doi:10.1890/06-0922.1.

Foken, T., M. Göckede, M. Mauder, L. Mahrt, B. Amiro, and W. Munger (2004), Post-field data quality control, in *Handbook of Micrometeorology: A Guide for Surface Flux Measurement and Analysis*, edited by X. Lee et al., pp. 181-208, Kluwer Acad., Dordrecht, Netherlands, doi:10.1007/1-4020-2265-4_9.

Geissbühler, P., R. Siegwolf, and W. Eugster (2000), Eddy covariance measurements on mountain slopes: The advantages of surface-normal sensor orientation over a vertical set-up, Boundary Layer Meteorol., 96: 371-392, doi:10.1023/A:1002660521017.

Gómez-Delgado, F., O. Roupsard, G. le Maire, S. Taugourdeau, A. Pérez, M. van Oijen, P. Vaast, B. Rapidel, J.-M. Harmand, M. Voltz, J.-M. Bonnefond, P. Imbach, and R. Moussa (2011), Modelling the hydrological behaviour of a coffee agroforestry basin in Costa Rica, Hydrol. Earth Syst. Sci., 15, 369-392, doi:10.5194/hess-15-369-2011.

Hammerle, A., A. Haslwanter, M. Schmitt, M. Bahn, U. Tappeiner, A. Cernusca, and G. Wohlfahrt (2007), Eddy covariance measurements of carbon dioxide, latent and sensible energy fluxes above a meadow on a mountain slope, Boundary Layer Meteorol., 122, 397-416, doi:10.1007/s10546-006-9109-x.

Harman, I. N., and J. J. Finnigan (2013), Flow over a narrow ridge covered with a plant canopy: a comparison between wind-tunnel observations and linear theory, Boundary Layer Meteorol., 147(1), 1-20, doi:10.1007/s10546-012-9779-5.

Hendricks Franssen, H. J., et al. (2010), Energy balance closure of eddy-covariance data: A multisite analysis for European FLUXNET stations, Agric. For. Meteorol., 150, 1553-1567, doi:10.1016/j.agrformet.2010.08.005.

Hiller, R., M. J. Zeeman, and W. Eugster (2008), Eddy-covariance flux measurements in the complex terrain of an alpine valley in Switzerland, Boundary Layer Meteorol., 127, 449-467, doi:10.1007/s10546-008-9267-0.

Holst, T., J. Rost, and H. Mayer (2005), Net radiation balance for two forested slopes on opposite sides of a valley, Int. J. Biometeorol., 49(5), 275-284, doi:10.1007/s00484-004-0251-1.

Horst, T., and J. Weil (1992), Footprint estimation for scalar flux measurements in the atmospheric surface-layer, Boundary-Layer Meteorol., 59 (3), 279–296, doi:10.1007/BF00119817.

Humphreys, E., T. Black, G. Ethier, G. Drewitt, D. Spittlehouse, E. Jork, Z. Nesic, and N. Livingston (2003), Annual and seasonal variability of sensible and latent heat fluxes above a coastal Douglas-fir forest, British Columbia, Canada, Agric. For. Meteorol., 115, 109-125, doi:10.1016/S0168-1923(02)00171-5.

Kalma, J., T. McVicar, and M. McCabe (2008), Estimating land surface evaporation: A review of methods using remotely sensing surface temperature data, Surv. Geophys., 29, 421-469, doi:10.1007/s10,712-008-9037-z.

Khlifi, S., M. Ameur, N. Mtimet, N. Ghazouani, and N. Belhadj (2010), Impacts of small hill dams on agricultural development of hilly land in the Jendouba region of northwestern Tunisia, Agric. Water Manage., 97(1), 50-56, doi:10.1016/j.agwat.2009.08.010.

Kool, D., N. Agam, N. Lazarovitch, J. Heitman, T. Sauer, and A. Ben-Gal (2014), A review of approaches for evapotranspiration partitioning, Agric. For. Meteorol., 184, 56-70, doi:10.1016/j.agrformet.2013.09.003.

Kustas, W. P., K. S. Humes, J. M. Norman, and S. M. Moran (1996), Single- and dual-source modeling of surface energy fluxes with radiometric surface temperature, J. Appl. Meteorol., 35(1), 110-121, doi:10.1175/1520-0450(1996)035<0110:SADSMO>2.0.CO;2.

Lee, X., J. J. Finnigan, and K. T. Paw (2004), Coordinate systems and flux bias error, in *Handbook of Micrometeorology: A Guide for Surface Flux Measurement and*

Analysis, edited by X. Lee et al., pp. 33-66, Kluwer Acad., Dordrecht, Netherlands, doi:10.1007/1-4020-2265-4_3.

Leuning, R., E. van Gorsel, W. J. Massman, and P. R. Isaac (2012), Reflections on the surface energy imbalance problem, Agric. For. Meteorol., 156, 65-74, doi:10.1016/j.agrformet.2011.12.002.

Liu, L., T. Wang, Z. Sun, Q. Wang, B. Zhuang, Y. Han, and S. Li (2012), Eddy covariance tilt corrections over a coastal mountain area in South-east China: significance for near-surface turbulence characteristics, Adv. Atmos. Sci., 29(6), 1264-1278, doi:10.1007/s00376-012-1052-9.

Maeda, E. E., P. J. Pellikka, M. Siljander, and B. J. Clark (2010), Potential impacts of agricultural expansion and climate change on soil erosion in the Eastern Arc Mountains of Kenya, Geomorphology, 123(3-4), 279-289, doi:10.1016/j.geomorph.2010.07.019.

Malone, S. L., C. L. Staudhammer, H. W. Loescher, P. Olivas, S. F. Oberbauer, M. G. Ryan, J. Schedlbauer, and G. Starr (2014), Seasonal patterns in energy partitioning of two freshwater marsh ecosystems in the Florida Everglades, J. Geophys. Res. Biogeosci., 119, 1487-1505, doi:10.1002/2014JG002700.

Mauder, M., M. Cuntz, C. Dre, A. Graf, C. Rebmann, H.P. Schmid, M. Schmidt, and R. Steinbrecher (2013), A strategy for quality and uncertainty assessment of long-term eddy-covariance measurements. Agric. For. Meteorol., 169, 122 – 135, doi:10.1016/j.agrformet.2012.09.006.

Mekki, I., J. Albergel, N. Ben Mechlia, and M. Voltz (2006), Assessment of overland flow variation and blue water production in a farmed semi-arid water harvesting catchment, Phys. Chem. Earth, 31(17), 1048-1061, doi:10.1016/j.pce.2006.07.003.

Mishra, S. K., R. Sarkar, S. Dutta, and S. Panigrahy (2008), A physically based hydrological model for paddy agriculture dominated hilly watersheds in tropical region, J. Hydrol., 357, 389-404, doi:10.1016/j.jhydrol.2008.05.019.

Moussa, R., N. Chahinian, and C. Bocquillon (2007), Distributed hydrological modelling of a Mediterranean mountainous catchment - Model construction and multi-site validation, J. Hydrol., 337(1-2), 35-51, doi:10.1016/j.jhydrol.2007.01.028.

Olioso, A., et al. (2002), Monitoring energy and mass transfers during the Alpilles-ReSEDA experiment, Agronomie, 22, 597–611, doi:10.1051/agro:2002051.

Pattey, E., G. Edwards, I. B. Strachan, R. L. Desjardins, S. Kaharabata, and C. W. Riddle (2006), Towards standards for measuring greenhouse gas fluxes from agricultural fields using instrumented towers, Can. J. Soil Sci., 86(3), 373-400, doi:10.4141/S05-100.

Patton E. G. and G. G. Katul (2009), Turbulent pressure and velocity perturbations induced by gentle hills covered with sparse and dense canopies, Boundary Layer Meteorol., 133(2), 189-217, doi:10.1007/s10546-009-9427-x.

Poggi, D., and G. G. Katul (2007), An experimental investigation of the mean momentum budget inside dense canopies on narrow gentle hilly terrain, Agric. For. Meteorol., 144, 1-13, doi:10.1016/j.agrformet.2007.01.009.

Poggi, D., G. G. Katul, J. J. Finnigan, and S. E. Belcher (2008), Analytical models for the mean flow inside dense canopies on gentle hilly terrain, Q. J. R. Meteorol. Soc., 134, 1095-1112, doi:10.1002/qj.276.

Raclot, D. and J. Albergel (2006), Runoff and water erosion modelling using WEPP on a Mediterranean cultivated catchment, Phys. Chem. Earth, 31(17), 1038-1047, doi:10.1016/j.pce.2006.07.002.

Rana, G., R. M. Ferrara, N. Martinelli, P. Personnic, and P. Cellier (2007), Estimating energy fluxes from sloping crops using standard agrometeorological measurements and topography, Agric. For. Meteorol., 146, 116-133, doi:10.1016/j.agrformet.2007.05.010.

Rana, G., N. Katerji, R. M. Ferrara, and N. Martinelli (2011), An operational model to estimate hourly and daily crop evapotranspiration in hilly terrain: validation on wheat and oat crops, Theor. Appl. Climatol., 103(3-4), 413-426, doi:10.1007/s00704-010-0308-5.

Rannik, Ü. (1998), On the surface layer similarity at a complex forest site, J. Geophys. Res., 103(D8), 8685–8697, doi:10.1029/98JD00086.

Raupach, M. and J. Finnigan (1997), The influence of topography on meteorological variables and surface-atmosphere interactions, J. Hydrol., 190, 182-213, doi:10.1016/S0022-1694(96)03127-7.

Rebmann, C., et al. (2005), Quality analysis applied on eddy covariance measurements at complex forest sites using footprint modelling, Theor. Appl. Climatol., 80, 121–141, doi:10.1007/s00704-004-0095-y.

Rebmann, C., O. Kolle, B. Heinesch, R. Queck, A. Ibrom, and M. Aubinet (2012), Data Acquisition and Flux Calculations, *In: Aubinet, Marc and Vesala, Timo and Papale, Dario (Ed.), Eddy Covariance*, pp. 59–83, Springer Atmospheric Sciences, Springer, Netherlands.

Ross, A., S. Arnold, S. Vosper, S. Mobbs, N. Dixon, and A. Robins (2004), A comparison of wind-tunnel experiments and numerical simulations of neutral and stratified flow over a hill, Boundary Layer Meteorol., 113(3), 427-459, doi:10.1007/s10546-004-0490-z.

Ross, A. N., and S. B. Vosper (2005), Neutral turbulent flow over forested hills, Q. J. R. Meteorol. Soc., 131, 1841-1862, doi:10.1256/qj.04.129.

Saha, R., P. K. Ghosh, V. K. Mishra, and K. M. Bujarbaruah (2007), Low-cost micro-rainwater harvesting technology (Jalkund) for new livelihood of rural hill farmers, Curr. Sci. 92(9), 1258-1265.

Scott, R. L. (2010), Using watershed water balance to evaluate the accuracy of eddy covariance evaporation measurements for three semiarid ecosystems, Agric. For. Meteorol., 150(2), 219-225, doi:10.1016/j.agrformet.2009.11.002.

Shao, C., J. Chen, L. Li, W. Xu, S. Chen, T. Gwen, J. Xu, and W. Zhang (2008), Spatial variability in soil heat flux at three Inner Mongolia steppe ecosystems, Agric. For. Meteorol., 148(10), 1433-1443, doi:10.1016/j.agrformet.2008.04.008.

Steeneveld, G. J., L. F. Tolk, A. F. Moene, O. K. Hartogensis, W. Peters, and A. A. M. Holtslag (2011), Confronting the WRF and RAMS mesoscale models with innovative observations in the Netherlands: Evaluating the boundary layer heat budget, J. Geophys. Res., 116, D23114, doi:10.1029/2011JD016303.

Tamura, T., A. Okuno, and Y. Sugio (2007), LES analysis of turbulent boundary layer over 3D steep hill covered with vegetation, J. Wind Eng. Ind. Aerodyn., 95, 1463-1475, doi:10.1016/j.jweia.2007.02.014.

Turnipseed, A. A., D. E. Anderson, P. D. Blanken, W. M. Baugh, and R. K. Monson (2003), Airflows and turbulent flux measurements in mountainous terrain. Part 1: Canopy and local effects, Agric. For. Meteorol., 119, 1-21, doi:10.1016/S0168-1923(03)00136-9.

van Dijk, A., A. Moene, and H. DeBruin (2004), The principles of surface flux physics: theory, practice and description of the ECPACK library, *Internal report 2004/1, Tech. rep.*, 99 pp., Meteorology and Air Quality Group, Wageningen, the Netherlands. [Available online http://www.met.wau.nl/projects/jep/report/ecromp/].

Wang, G., J. Huang, W. Guo, J. Zuo, J. Wang, J. Bi, Z. Huang, and J. Shi (2010), Observation analysis of land-atmosphere interactions over the Loess Plateau of northwest China, J. Geophys. Res., 115, D00K17, doi:10.1029/2009JD013372.

Wang, K. C., and R. E. Dickinson (2012), A review of global terrestrial evapotranspiration: Observation, modeling, climatology, and climatic variability, Rev. Geophys., 50, RG2005, doi:10.1029/2011RG000373.

Wilczak, J. M., S. P. Oncley, and S. A. Stage (2001), Sonic anemometer tilt correction algorithms, Boundary Layer Meteorol., 99, 127-150, doi:10.1023/A:1018966204465.

Wilson, K., et al. (2002), Energy balance closure at FLUXNET sites, Agric. For. Meteorol., 113, 223–243, doi:10.1016/S0168-1923(02)00109-0.

Xu, Z., S. Liu, X. Li, S. Shi, J. Wang, Z. Zhu, T. Xu, W. Wang, and M. Ma (2013), Intercomparison of surface energy flux measurement systems used during the

HiWATER-MUSOEXE, J. Geophys. Res. Atmos., 118, 13,140-13,157, doi:10.1002/2013JD020260.

Zeri, M., C. Rebmann, C. Feigenwinter, and P. Sedlak (2010), Analysis of periods with strong and coherent CO2 advection over a forested hill, Agric. For. Meteorol., 150(5), 674-683, doi:10.1016/j.agrformet.2009.12.003.

Zeri, M., M. Z. Hussain, K. J. Anderson-Teixeira, E. DeLucia, and C. J. Bernacchi (2013), Water use efficiency of perennial and annual bioenergy crops in central Illinois, J. Geophys. Res. Biogeosci., 118, 581-589, doi:10.1002/jgrg.20052.

Zhang, Q. J., B. J. Fu, L. D. Chen, W. W. Zhao, Q. K. Yang, G. B. Liu, and H. Gulinck (2004), Dynamics and driving factors of agricultural landscape in the semiarid hilly area of the Loess Plateau, China, Agric. Ecosyst. Environ., 103(3), 535-543, doi:10.1016/j.agee.2003.11.007.

Zitouna-Chebbi, R., L. Prévot, F. Jacob, R. Mougou, and M. Voltz (2012), Assessing the consistency of eddy covariance measurements under conditions of sloping topography within a hilly agricultural catchment, Agric. For. Meteorol., 164, 123-135, doi:10.1016/j.agrformet.2012.05.010.

List of Figures

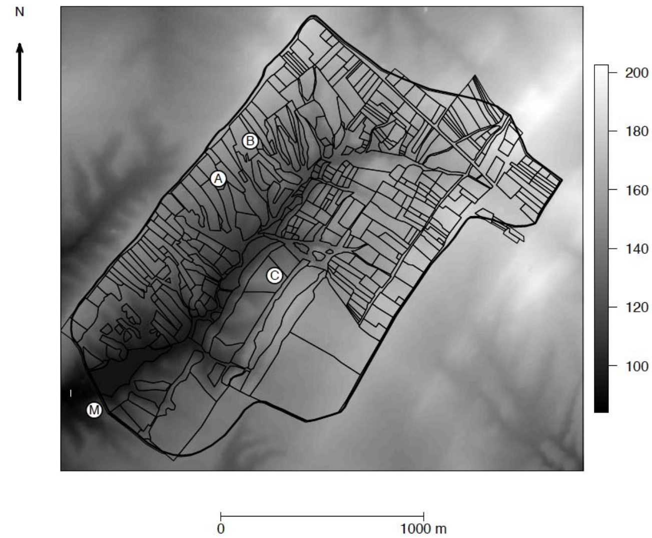

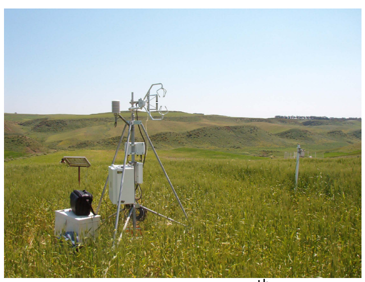
Field A, wheat, April 7th, 2004


Field B, oat, May 11th, 2006


Field A, pasture, June 1st, 2006


Field C, rangeland, May 18th, 2006

Figure 1: (top) Topography of the Kamech watershed deduced from a 4-m spatial resolution digital elevation model (DEM). Altitude above sea level is given in meters (right gray-scale bar). The thick black line represents the watershed outline, and the thin black lines represent the field limits. The white circles indicate the locations of the meteorological station (M) and of the flux stations on fields A, B and C. (Middle and bottom) Pictures of each experimental setup within field A in 2004, field B in 2005, field A in 2006 and field C in 2006.

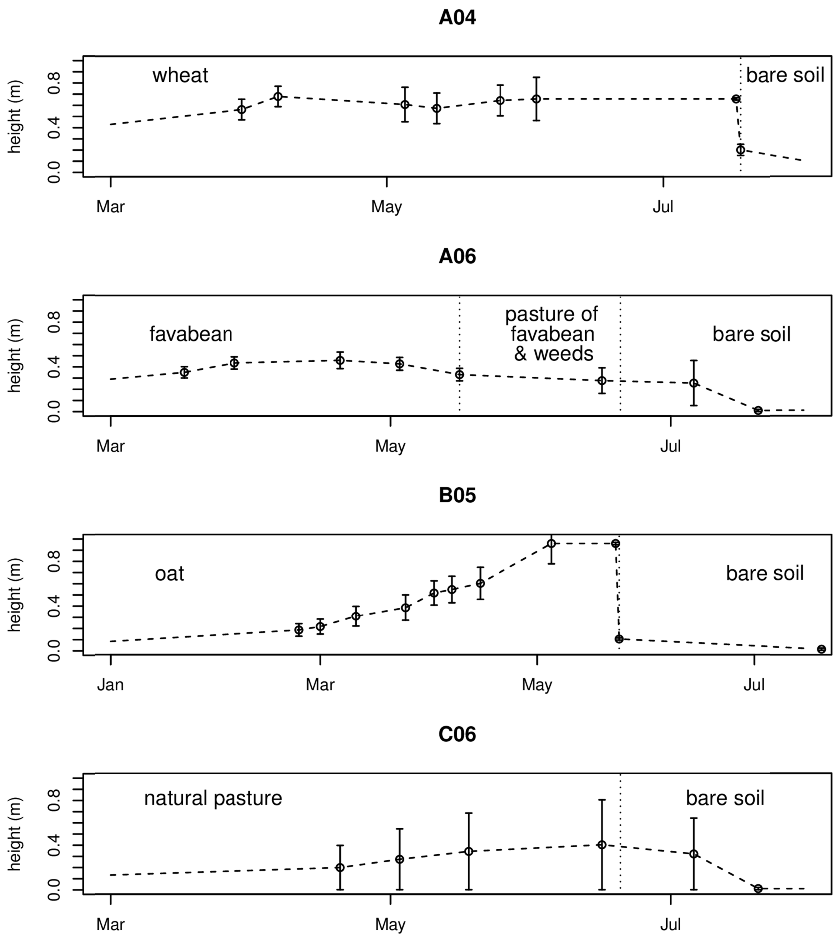

Figure 2: Chronicles of vegetation height *hv*. From top to bottom are sub-plotted estimates for field A in 2004, field A in 2006, field B in 2005 and field C in 2006. Points represent averaged values of vegetation height measurements over the samples collected within a given field on a given day. Vertical bars represent standard deviations over the samples. Dashed lines represent temporally interpolated values. Vertical dotted lines indicate specific changes detailed hereafter. Vertical dotted lines in subplot A04 and B05 represent the harvest times. First vertical dotted line in subplot A06 represents the harvest time and the subsequent start of the pasture period (only beans were harvested, no vegetation cut). Second vertical dotted line in subplot A06 and vertical dotted line in subplot C06 represent the start of periods with very sparse vegetation.

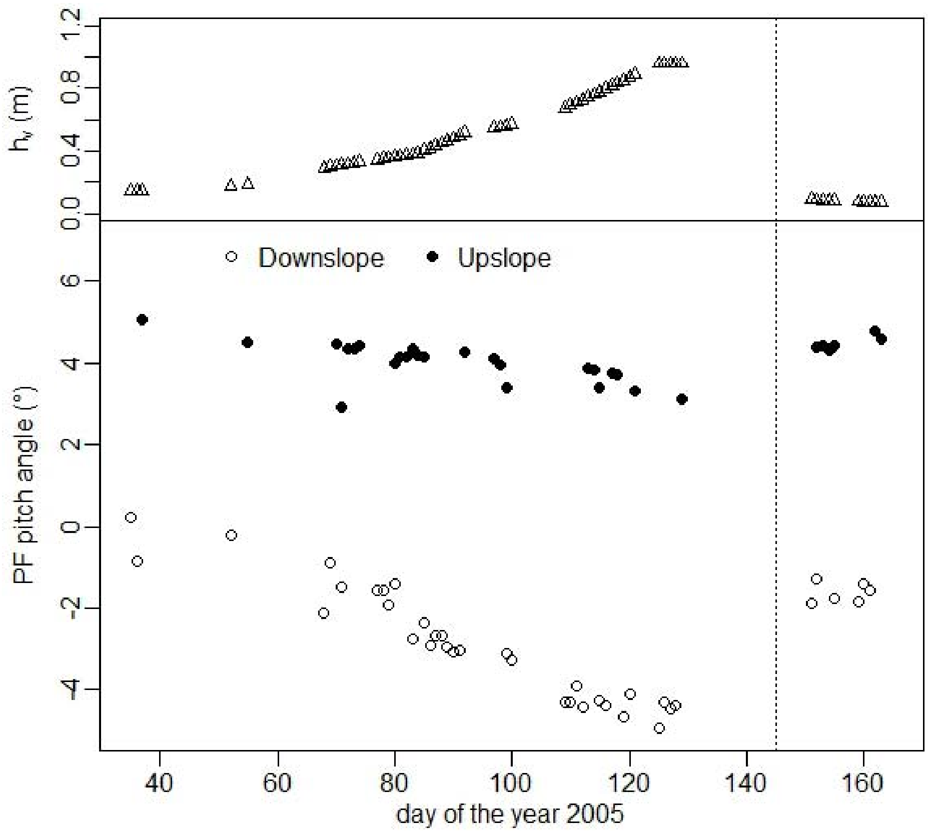

Figure 3: Temporal evolutions of vegetation height *hv* (top subplot), and of planar fit (PF) pitch angle (bottom subplot) for upslope winds (solid circles) and downslope winds (opened circles). Vertical dotted lines indicate the harvest date. Measurements from the B05 dataset, with downslope winds from north and upslope winds from south.

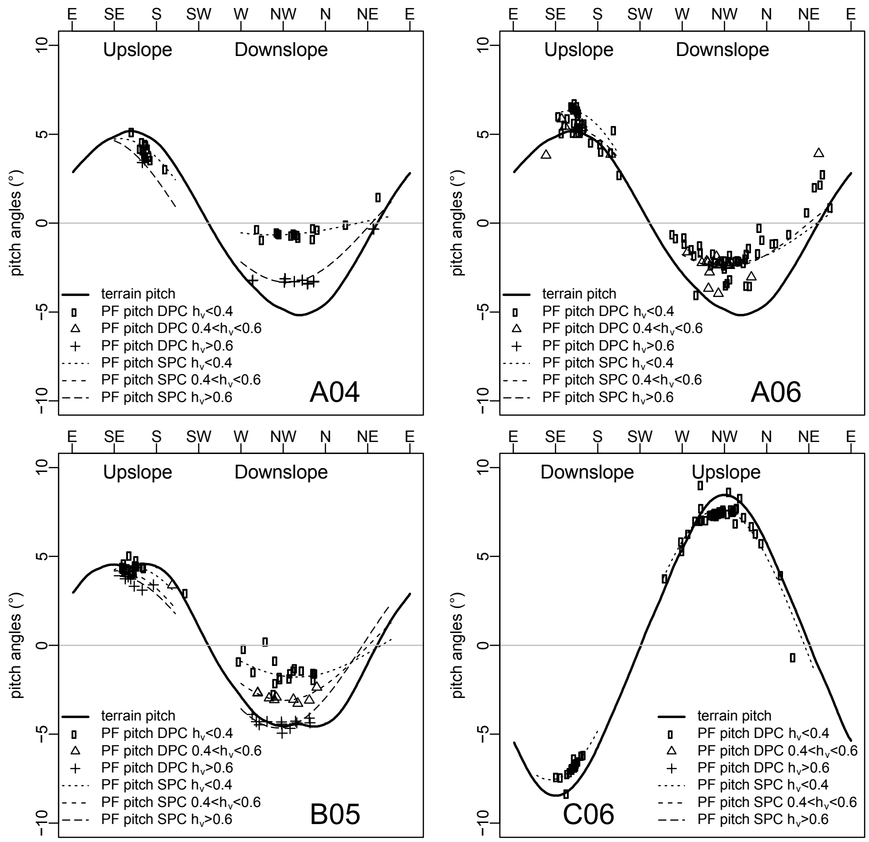

Figure 4: Compared evolution of the planar fit derived pitch angles and the terrain pitch angles (y-axis) with respect to the wind direction (x-axis, 0° is north, 90° is east) for dataset A04 (top left subplot), A06 (top right subplot), B05 (bottom left subplot) and C06 (bottom right subplot). The continuous curves represent the terrain pitch angle, as derived from the DEM data. The planar fit-derived pitch angles evaluated for each day and each wind sector (labeled PF pitch DPC for daily plane calculation) are represented by symbols (circles if $hv \in [0 – 0.4[$, triangles if $hv \in [0.4 – 0.6[$, and crosses if $hv \in [0,6 – 1[$, with hv in meters). The planar fit derived pitch angles for all of the data belonging to both a given wind sector and a given hv interval (labeled PF pitch SPC for single plane calculation) are represented with portions of discontinuous curves (long dashed if $hv \in [0 – 0.4[$, short dashed if $hv \in [0.4 – 0.6[$, and dotted if $hv \in [0,6 – 1[$, with hv in meters). In this last case, wind sectors (south and northwest) are indicated with x-axis.

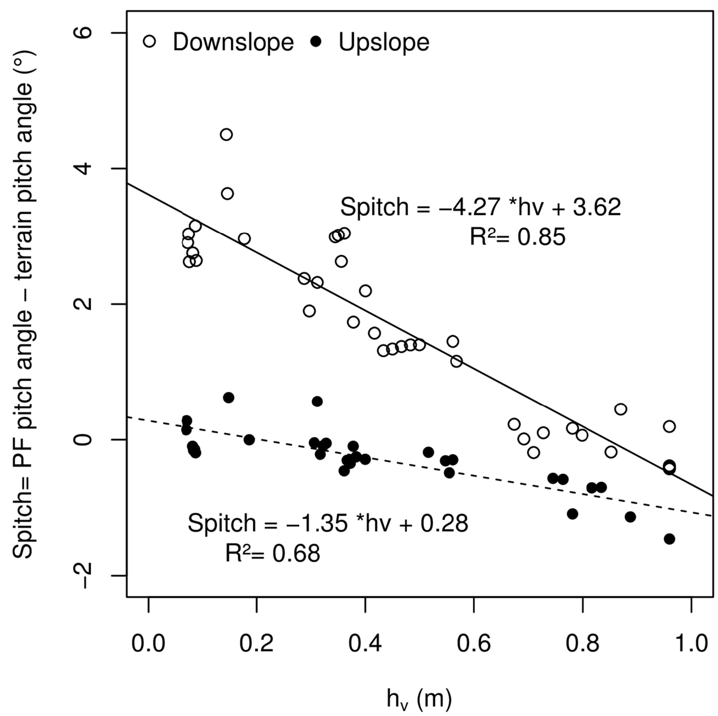

Figure 5: Characterization of the shifted pitch angle (defined as the difference between PF pitch angle and terrain pitch angle) as a function of the vegetation height *hv*. We considered the B05 dataset that spread over the vegetation growth cycle. Continuous line is the regression line over the data corresponding to downslope winds (opened circles). Dashed line is the regression line over the data corresponding to upslope winds (solid circles).

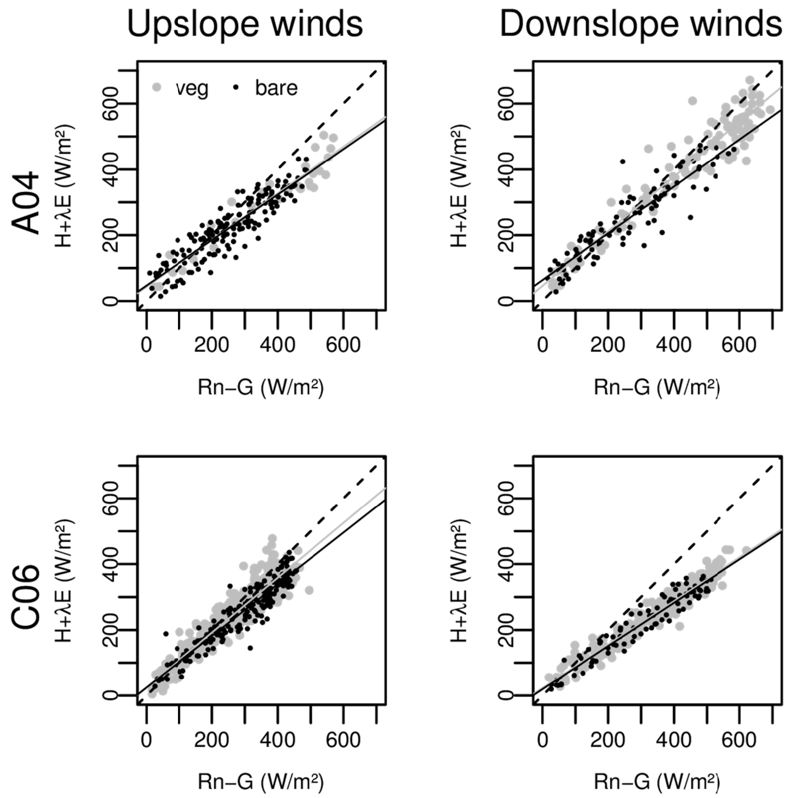

Figure 6: Energy balance closure analysis that compares the convective fluxes $CF = H + \lambda E$ (y-axis) against the available energy $AE = Rn - G$ (x-axis). The left column corresponds to upslope winds and the right column corresponds to downslope winds. The first line corresponds to the dataset A04, and the second line corresponds to the dataset C06. We selected conditions of both bare soil (black circles labeled "bare" in legend) and vegetation cover (gray circles labeled "veg" in legend). Each symbol corresponds to a 30-minute interval measurement. For each scatterplot, the dashed line is the 1:1 line, and the continuous line is the y-axis data versus x-axis data regression line (regression coefficients are given in Table 3).

List of Tables

Table 1: Presentation of the experimental conditions for the four datasets

Dataset label	Field label	Land use	Measurement period	Phenological stage	Maximum vegetation height (m)
A04	A	Durum wheat	30/03/04 ➔ 16/07/04	From heading to yellow ripeness	0.68
			17/07/04	Harvest	
		Bare soil	18/07/04 ➔ 04/11/04	-	
A06	A	Favabean	03/03/06 ➔ 15/05/06	Full development	0.46
			16/05/06	Harvest	
		Favabean and weeds	17/05/06 ➔ 20/06/06	Senescence	
		Bare soil	21/06/06 ➔ 28/07/06	-	
B05	B	Oat	18/01/05 ➔ 24/05/05	From emergence to heading	0.96
			25/05/05	Harvest	
		Bare soil	26/05/05 ➔ 20/06/05	-	
C06	C	Rangeland	13/04/06 ➔ 20/06/06	From greenness to senescence	0.40
		Bare soil	21/06/06 ➔ 27/07/06	-	

Table 2: Listing of the instruments, acquisition and storage frequency for each flux station

Instrument type	field A Year 2004	field A Year 2006	field B Year 2005	field C Year 2006	Acquisition frequency	Storage frequency
Datalogger	CR23X (Campbell Scientific Inc., USA)					
Net radiometer	NR-lite (Kipp & Zonen, the Netherlands)				1 s	30 mn
Soil heat flux sensors	HFP01 (Hukseflux, the Netherlands) (three per field)				1 s	30 mn
Thermo-hygrometer probe	HMP45C (Vaisala, Finland)				1 s	30 mn
Sonic anemometer	CSAT3 (Campbell Scientific Inc., USA)			Young-81000V (R.M. Young, USA)	10 Hz	10 Hz
Krypton hygrometer	KH20 (Campbell Scientific Inc., USA)	(KH20 was off)		KH20 (Campbell Scientific Inc., USA)	10 Hz	10 Hz

Table 3: Statistical indicators for characterizing the energy balance closure [a]

	Conditions of bare soil				Conditions of vegetation cover			
	A04		C06		A04		C06	
	Up	Down	Up	Down	Up	Down	Up	Down
N	155	99	233	120	32	132	328	240
Slope *a*	0.69	0.71	0.73	0.64	0.71	0.83	0.83	0.66
Offset *b* (W m^{-2})	47.0	63.3	44.8	28.2	43.3	46.0	25.1	23.0
R^2	0.82	0.84	0.88	0.93	0.92	0.93	0.88	0.95
RMSD (W m^{-2})	63.7	65.5	55.6	100.9	87.4	62.6	44.7	110.8
URMSD (W m^{-2})	39.6	47.4	34.9	25.6	38.0	46.8	35.8	23.3
EBRAT (W m^{-2})	0.87	0.95	0.90	0.73	0.83	0.94	0.93	0.73
EBRES (W m^{-2})	32.7	12.2	26.9	81.2	61.3	25.1	19.0	96.0

[a] We compare the convective fluxes CF ($CF = H + \lambda E$) as the y-axis variable against the available energy AE ($AE = Rn - G$) as the x-axis variables. N is the number of data (30-minute intervals). Terms a and b are, respectively, the slope and the intercept of the $y = a\ x + b$ linear regression (gray and black continuous lines for vegetation and bare soil, respectively, in Figure 6). R^2 is the coefficient of determination between y and x. *RMSD* is the root mean square difference between y and x. *URMSD* is the unsystematic *RMSD*, defined as the scattering around the $y = a\,x + b$ linear regression. *EBRAT* is the energy balance ratio defined as $EBRAT = CF / AE$. *EBRES* is the energy balance residual, defined as $EBRES = AE - CF$. Label "Up" is for upslope winds, and label "Down" is for downslope winds. The metrics used here were selected from among those reviewed by Kustas et al. (1996) and Wilson et al. (2002). The results for bare soil are from Zitouna-Chebbi et al. (2012).

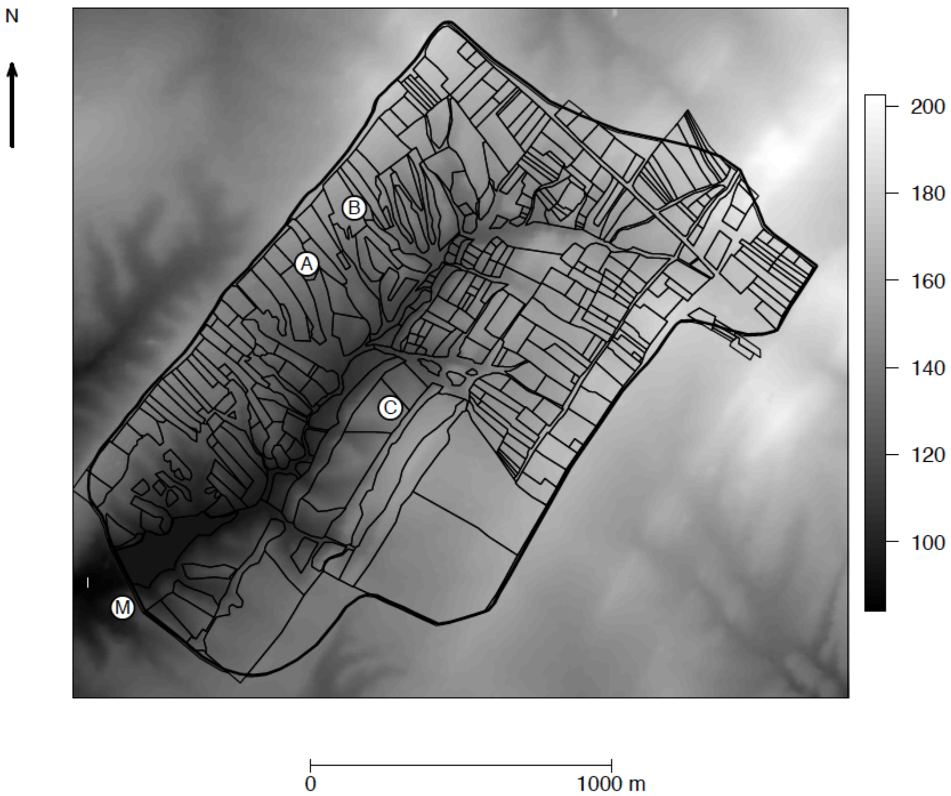

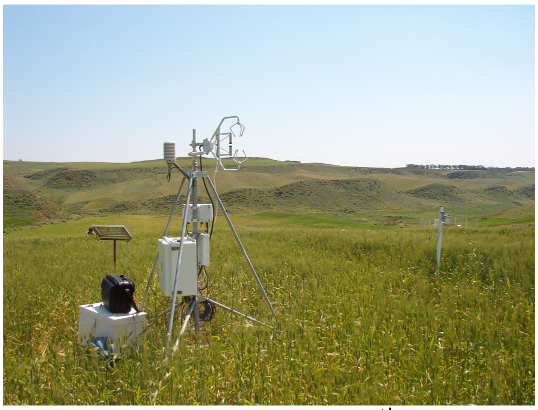

Field A, wheat, April 7th, 2004

Field B, oat, May 11th, 2006

Field A, pasture, June 1st, 2006

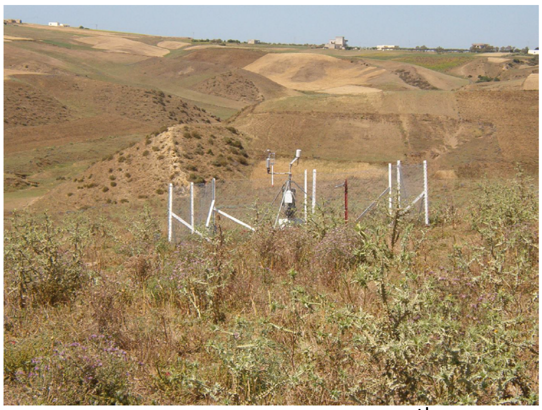

Field C, rangeland, May 18th, 2006

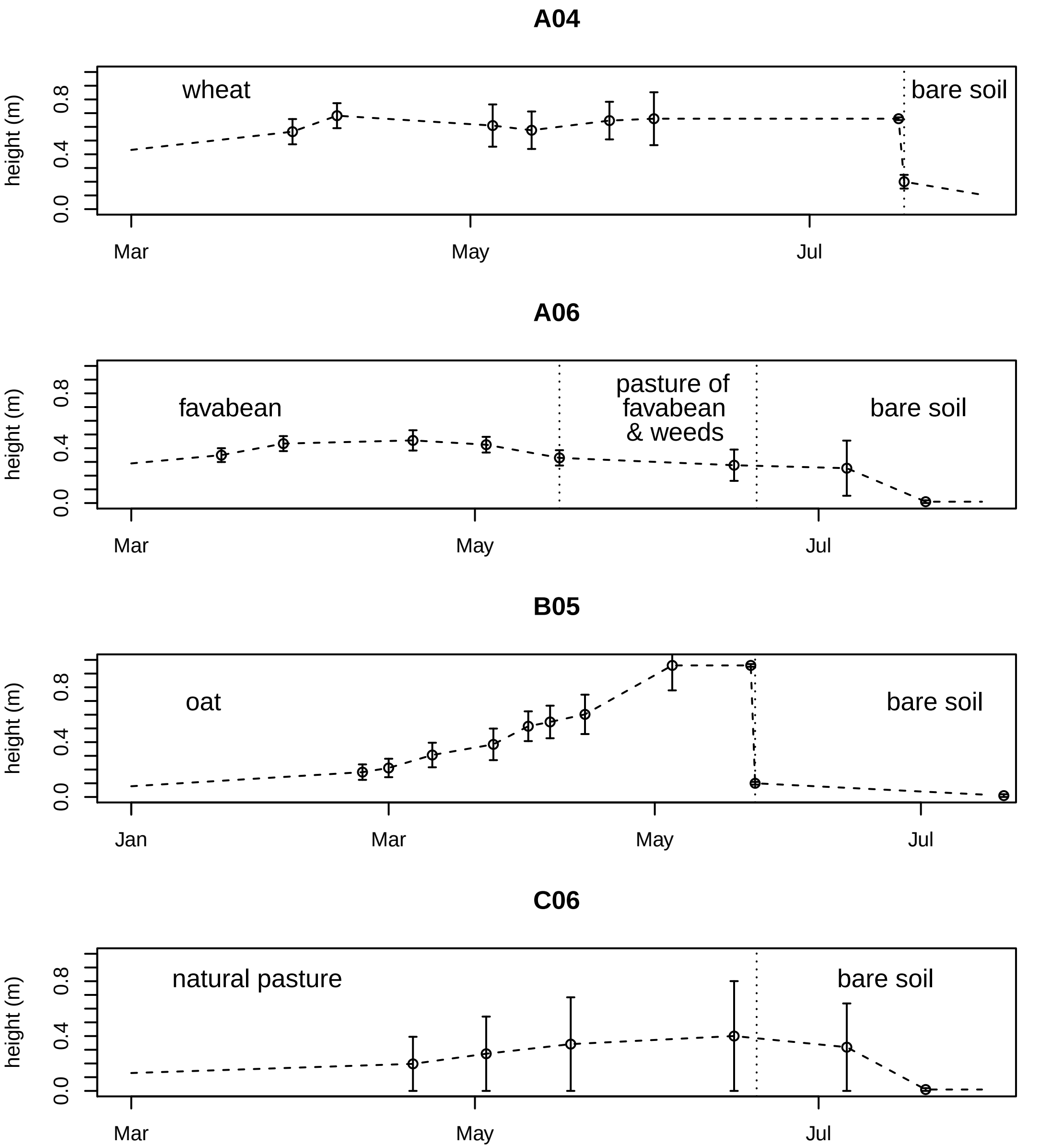
A04
wheat
bare soil
height (m)
0.0
0.4
0.8
Mar
May
Jul
A06
favabean
pasture of
favabean
& weeds
bare soil
height (m)
0.0
0.4
0.8
Mar
May
Jul
B05
oat
bare soil
height (m)
0.0
0.4
0.8
Jan
Mar
May
Jul
C06
natural pasture
bare soil
height (m)
0.0
0.4
0.8
Mar
May
Jul

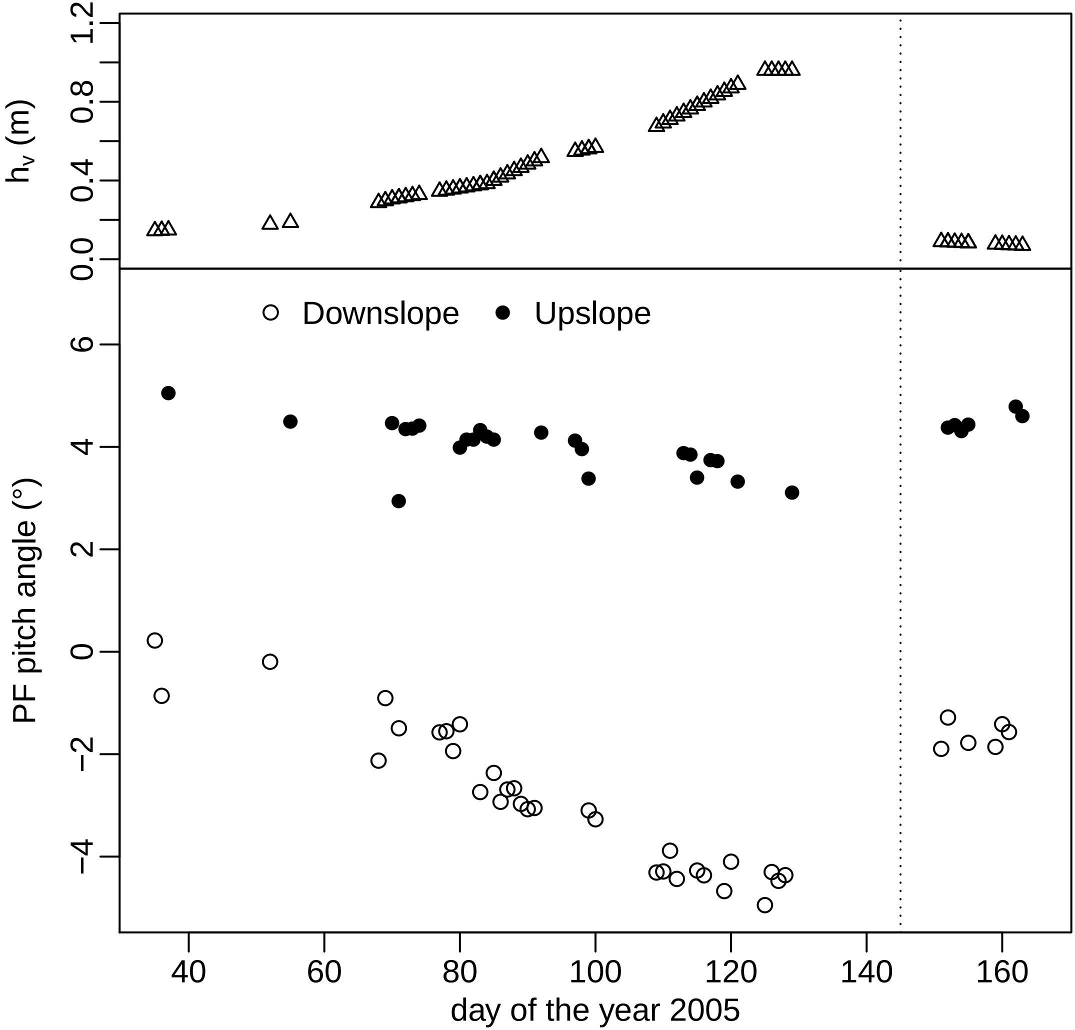

1.2
0.8
0.4
0.0
h_v (m)
Downslope
Upslope
6
4
2
0
−2
−4
PF pitch angle (°)
40
60
80
100
120
140
160
day of the year 2005

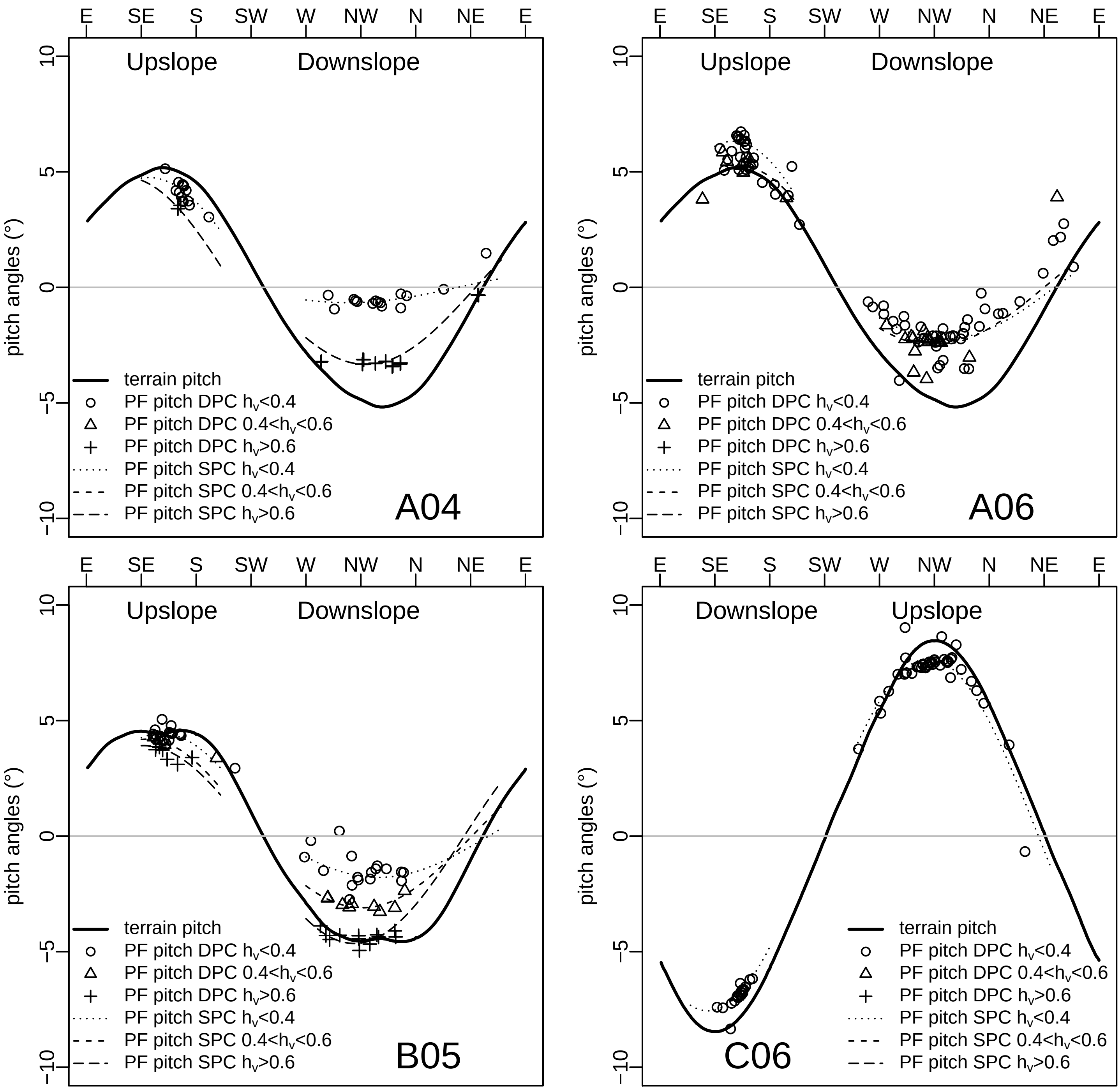
E SE S SW W NW N NE E
Upslope
Downslope
pitch angles (°)
10
5
0
−5
−10
terrain pitch
PF pitch DPC h_v<0.4
PF pitch DPC 0.4<h_v<0.6
PF pitch DPC h_v>0.6
PF pitch SPC h_v<0.4
PF pitch SPC 0.4<h_v<0.6
PF pitch SPC h_v>0.6
A04
A06
B05
C06

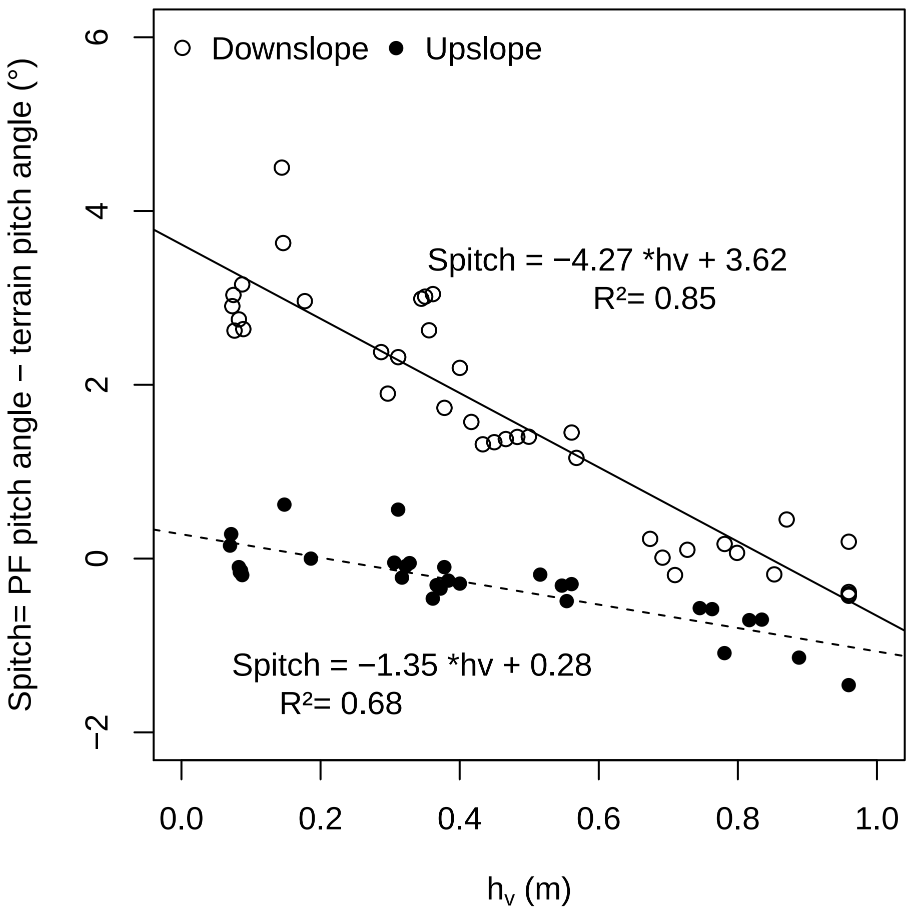

Downslope
Upslope
Spitch = −4.27 *hv + 3.62
R²= 0.85
Spitch = −1.35 *hv + 0.28
R²= 0.68
Spitch= PF pitch angle − terrain pitch angle (°)
hv (m)
−2
0
2
4
6
0.0
0.2
0.4
0.6
0.8
1.0

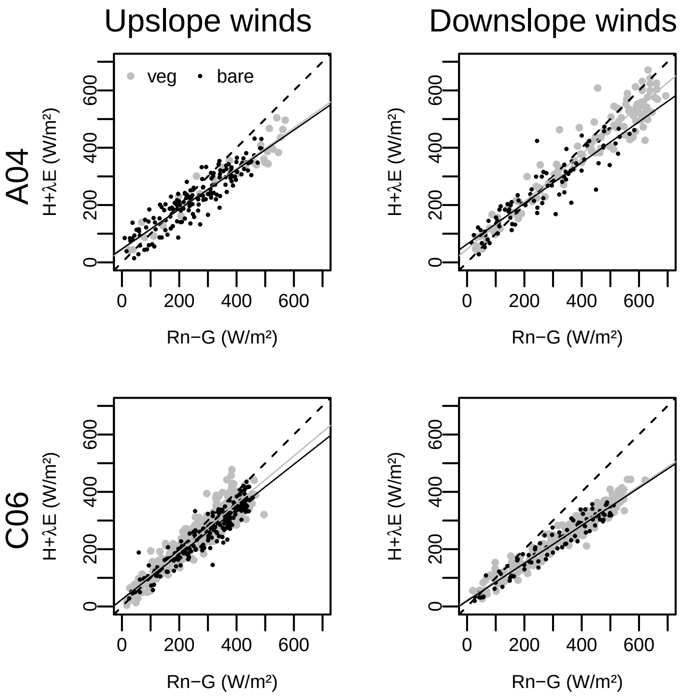

Upslope winds
Downslope winds
A04
C06
veg
bare
H+λE (W/m²)
Rn−G (W/m²)
0
200
400
600